Supporting Information

Spielberg et al. 10.1073/pnas.1500048112

SI Materials and Methods

Participants. A total of 120 participants were recruited from the community. Exclusion criteria were as follows: claustrophobia, left-handedness, prior serious brain injury, abnormal hearing/vision, metal in body, pregnancy, and nonnative English. Data from 19 participants were not used because of movement ≥3.3 mm relative to the middle volume or ≥2 mm relative to the previous volume, ≥15% task errors, significant signal loss due to susceptibility artifact, and/or serious motion-related activation patterns. The final sample size was 101 (63% female, mean age = 34.2 y, range 19–51 y).

Color-Word Stroop Task. A total of 256 trials were presented in 16 blocks (4 congruent, 4 incongruent, and 8 neutral), with a variable intertrial interval (2,000 ± 225 ms). Additional neutral trials were intermixed 50:50 in congruent and incongruent blocks to prevent the development of word-reading strategies. Each trial consisted of one word presented in one of four ink colors, with each color occurring equally often with each word type. Word meaning was the same as ink color in congruent trials (e.g., "RED" in red ink), whereas word meaning differed from ink color in incongruent trials (e.g., "GREEN" in red ink), and the two were unrelated in neutral trials (e.g., "LOT" in red ink). Task condition alternated by block, and order was counterbalanced.

Acquisition. fMRI data were 370 EPI images (duration = 12.33 min, repetition time = 2,000 ms, echo time = 25 ms, flip angle = 80°, field of view = 220 cm), each consisting of 38 axial slices (slice thickness = 3 mm, 0.3 mm gap, resolution = 3.4375 × 3.4375 mm), acquired on a Siemens 3T Trio scanner, along with a 1-mm^3 anatomical acquisition.

Preprocessing. Data were preprocessed primarily via the GTG toolbox. Data were motion-corrected, field map-corrected (via FSL's Fugue), despiked (via AFNI's 3dDespike), and second-order detrended, and each participant's mean global, ventricular, and white-matter signals were partialled out, along with estimated motion parameters. To ensure that task effects were not artificially inflating connectivity estimates, analyses were recomputed after first partialling condition-related responses from the full time series (after preprocessing, but before deconvolution). The resultant connectivity estimates were virtually identical, and all findings remained significant.

Creation of Connectivity Matrices. A 130 ROI atlas was used [created by Craddock et al. (45) via two-level spatially constrained spectral clustering]. ROIs in cerebellum (n = 16) were removed, due to inconsistent spatial coverage of cerebellum during acquisition. Time series for each ROI were extracted by calculating the mean (across voxels) signal per time point. Each time series was deconvolved for the HDR via SPM's method. Time series were divided by block; blocks were concatenated by condition; and a 114 × 114 Pearson correlation matrix was created for each participant separately for each condition.

Follow-Up Analyses to Rule Out Bias due to Atlas Choice. To ensure that our choice of atlas did not bias findings, analyses were recomputed by using a Craddock et al. atlas with 50% more ROIs (total number of ROIs = 171 after cerebellum removal). A similar network was observed in the NBS analyses (Fig. S1). In addition, all graph property findings were significant using this new atlas.

Follow-Up Analyses to Rule Out Bias due to Thresholding to Include Only Positive Weights. To ensure that the use of only a single threshold (to include only positive weights) did not bias findings, graph properties were recomputed across a series of density thresholds by using the GTG toolbox. A minimum density of 0.23 was chosen, because this value was the lowest threshold at which all nodes remained (at least indirectly) connected in a set of mean matrices (mean across participants within each condition and mean across conditions). A maximum density of 0.60 was used along with a step size between densities of 0.01, resulting in 38 density thresholds examined. Graph properties were calculated for each threshold, and the area under the curve was computed to create one value per property. This procedure (using series of densities) was used to ensure that findings were not biased by the choice of a single, arbitrary threshold. Importantly, all analyses remained significant when using this alternate set of graph properties.

Modularity Assignment. Modularity was computed on the mean network by using the Louvain algorithm followed by the Kernighan–Lin fine-tuning algorithm (10,000 repetitions, modularization with the highest modularity chosen; see Table S1 for module structure). Given that a condition with higher overall connectivity (e.g., incongruent) could bias module assignment, we computed modularity using data from the neutral condition.

Relationships with Behavior. For RT and error rate, difference scores were divided by the sum of incongruent and congruent to remove individual differences in mean RT/errors. To ensure that outliers did not drive findings, data were winsorized to 2.5 SDs from the mean.

Exploratory analyses were also conducted by using drift rate and boundary distance derived from a variant of the EZ-Diffusion model (46). Drift rate is thought to reflect the ability of the participant to exhibit inhibitory control, whereas boundary distance is thought to reflect the conservativeness of the response criterion (the amount of information/confidence needed before responding). For this model, mean starting point, z, was assumed to be 0.25 instead of 0.5 to account for the fact that four response options were possible, only one of which (i.e., 0.25) was correct on a given trial. Findings revealed negative correlations between several network parameters and (incongruent vs. congruent) boundary distance: mean NBS network connection strength (r = −0.205, P = 0.048), global efficiency (r = −0.227, P = 0.029), transitivity (r = −0.227, P = 0.028), right IFS node strength (r = −0.290, P = 0.005), right AI node strength (r = −0.257, P = 0.013), right IFS local efficiency (r = −0.265, P = 0.010), and right IFS participation coefficient (r = −0.236, P = 0.023). No network parameters correlated with drift rate. See Fig. S2 for scatterplots of all relationships.

Incongruent vs. Neutral. To ascertain whether a similar pattern of findings emerged when the neutral condition was used as a baseline instead of congruent, NBS and GTG analyses were recomputed, substituting in the neutral condition.

SI Results

Higher demand for inhibitory control (i.e., incongruent > neutral) was associated with stronger coupling in a network (order 21, size 31; Fig. S3) that overlapped the network found when congruent was used as a baseline. Node-specific topological properties were tested for the three regions examined for

incongruent vs. congruent, along with right IFGpo, given that this region exhibited the largest number of differential connections when using neutral as a baseline. Similar to the analyses using congruent as a baseline, higher demand for inhibitory control (i.e., incongruent > neutral) was associated with increases in transitivity ($P < 0.001$ [< 0.001]) and global efficiency ($P < 0.001$ [< 0.001]); greater node strength for medial dACC ($P < 0.001$ [< 0.001]), right IFS ($P < 0.001$ [$<. 001$]), and right AI ($P < 0.001$ [< 0.001]); greater local efficiency for medial dACC ($P < 0.001$ [< 0.001]), right IFS ($P < 0.001$ [< 0.001]), and right AI ($P < 0.001$ [< 0.001]); stronger within-module degree Z-score for medial dACC ($P = 0.002$ [0.024]); and increased participation coefficient for right AI ($P = 0.034$ [0.347]), although this last effect did not survive correction for multiple comparisons. The only effects not present when using neutral as a baseline were higher assortativity and participation coefficient for right IFS.

An additional effect emerged that was not present when using congruent as a baseline. Specifically, higher demand for inhibitory control was associated with stronger within-module degree Z-score for right IFS ($P = 0.002$ [0.016]). Several effects also emerged for the additional node examined, right IFGpo: greater node strength ($P < 0.001$ [< 0.001]) and local efficiency ($P < 0.001$ [< 0.001]) and weaker within-module degree Z-score ($P = 0.003$ [0.024]).

Regional Task Activation Methods.

Preprocessing. Image processing and statistical analysis was implemented primarily via FSL's FEAT. Functional data for each participant were motion-corrected, intensity-normalized, temporally high-pass filtered, and spatially smoothed (FWHM = 5 mm). Temporal low-pass filtering was carried out by using AFNI's 3dDespike.

First-Level Data Processing. Regression analyses were performed voxel-wise on the processed functional time series. Four HDR-convolved predictors, one for each word type block (congruent, incongruent, and neutral) and one modeling the rest condition, were included. The comparison of interest was the contrast of the incongruent with the congruent condition. Functional data were nonlinearly warped into the MNI152 nonlinear template via FNIRT.

Group-Level Processing. Group inferential statistical analyses were carried out by using FLAME. The mean incongruent > congruent response across the sample was calculated via voxel-wise one-sample *t* tests. Gaussian-random-field correction for multiple comparisons was computed via FSL's Cluster, with voxel-level threshold of z = 4.

Regional Task Activation Results. Findings from the incongruent > congruent regional task activation analyses are provided in Table S2 and Fig. S4. Nodes present in both network and regional task activation analyses were medial dACC/paracingulate, right AI, bilateral IFGpo, left posterior MFG, right precentral, and medial precuneous. Nodes present in network, but not regional task activation, analyses were right IFS (although a nearby region of MFG is present, and activation extends into IFS at lower thresholds), left precentral, right posterior superior/middle temporal gyrus, left posterior superior frontal gyrus (SFG), right posterior MFG/precentral gyrus, and right amygdala/hippocampus. Nodes present in regional task activation, but not in network, analyses were left inferior frontal pole, bilateral angular gyrus, left posterior supramarginal gyrus, left AI, bilateral posterior orbitofrontal cortex, medial thalamus, bilateral superior parietal lobule, left inferior temporal gyrus temporooccipital part, bilateral superior lateral occipital cortex, and bilateral intracalcarine gyrus. See Fig. S5 for a depiction of overlap.

Activation in no regions correlated with incongruent vs. congruent RT. Activation in several regions correlated with incongruent vs. congruent error rate: left frontal pole ($r = 0.214$, $P = 0.039$), right angular gyrus ($r = 0.303$, $P = 0.003$), left intracalcarine cortex ($r = 0.299$, $P = 0.004$), IFGpo/precentral gyrus ($r = 0.226$, $P = 0.029$), right AI/posterior orbitofrontal cortex ($r = 0.313$, $P = 0.002$), medial dACC/posterior paracingulate ($r = 0.257$, $P = 0.013$), left AI/posterior orbitofrontal cortex/IFGpo/posterior MFG ($r = 0.259$, $P = 0.012$), left lateral occipital cortex/angular gyrus ($r = 0.223$, $P = 0.032$), and medial thalamus ($r = 0.239$, $P = 0.021$).

Several regions correlated with drift rate: left intracalcarine cortex ($r = -0.213$, $P = 0.040$), right AI/posterior orbitofrontal cortex ($r = -0.305$, $P = 0.003$), medial dACC/posterior paracingulate ($r = -0.292$, $P = 0.005$), and left AI/posterior orbitofrontal cortex/IFGpo/posterior MFG ($r = -0.261$, $P = 0.011$). Two regions correlated with boundary distance: right angular gyrus ($r = -0.249$, $P = 0.016$) and right insula/posterior orbitofrontal cortex ($r = -0.207$, $P = 0.047$).

Age Analyses. Supplementary analyses investigated whether age moderated task effects in behavior, brain networks (i.e., via the NBS toolbox), or graph properties (i.e., via the GTG toolbox). Specifically, the correlation between age and the incongruent vs. congruent difference score for mean RT/errors was computed. In addition, NBS and GTG analyses were recomputed, with the addition of age as a between-subject predictor. As well, the correlation between age and mean connection weight in the task-related network identified previously via NBS was computed. No significant effects were observed.

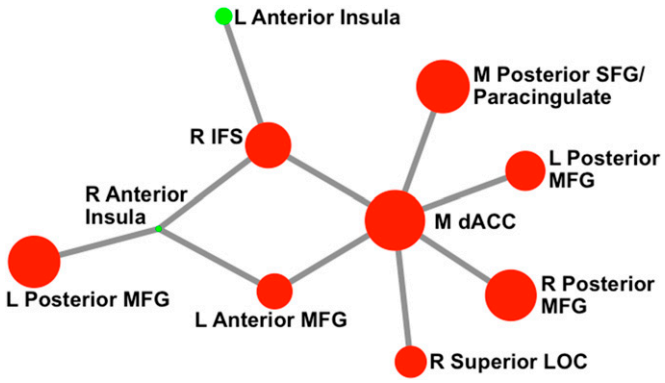

Fig. S1. Network that emerged for the 171 node atlas. Circle color represents module membership, and circle size reflects node strength (across conditions). This network representation was created by using the Kamada–Kawai spring embedder algorithm. Only links (and the corresponding nodes) that were identified in the NBS analyses as differing significantly by condition are shown above. M, medial; R, right; L, left; LOC, lateral occipital cortex.

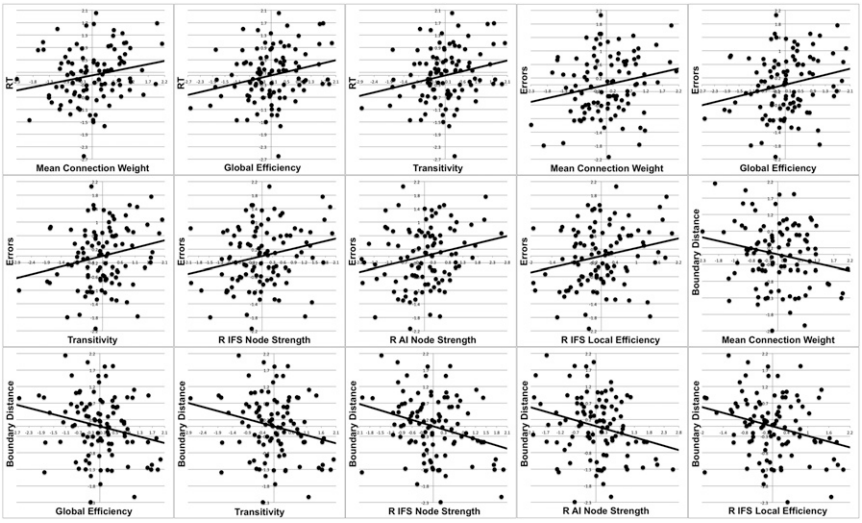

Fig. S2. Scatterplots of brain–behavior relationships. All variables are difference scores (incongruent – congruent) and have been residualized with respect to counterbalancing order and age. R, right.

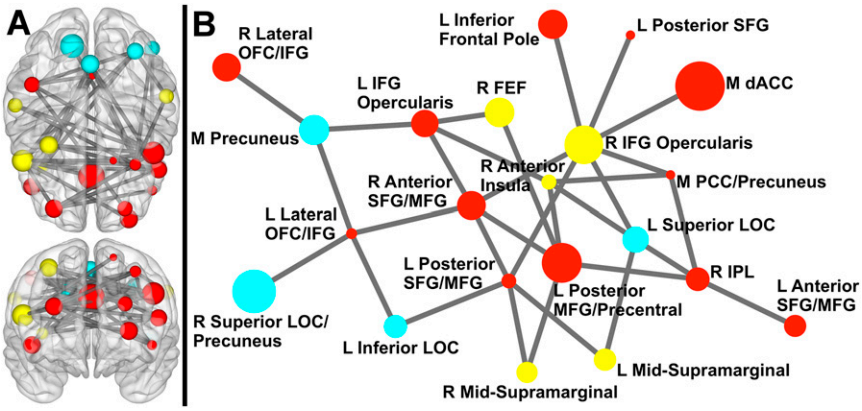

Fig. S3. Network exhibiting greater coupling for incongruent than neutral. (*A*) Sphere color represents module membership, and sphere size reflects node strength (across task conditions). *Upper* is a 3D axial view from above the brain; *Lower* is a 3D coronal view from anterior to the brain (to maintain the right side of the brain on the right side of the image for both views, posterior is positioned on top for the axial view). Sphere placement in the brain reflects the center of mass location of that node. (*B*) Circle color represents module membership and circle size reflects node strength. This network representation was created using the Kamada–Kawai spring embedder algorithm. Only links (and the corresponding nodes) that were identified in the NBS analyses as differing significantly by condition are shown above. FEF, frontal eye field; L, left; LOC, lateral occipital cortex; M, medial; OFC, orbitofrontal cortex; PCC, posterior cingulate cortex; R, right.

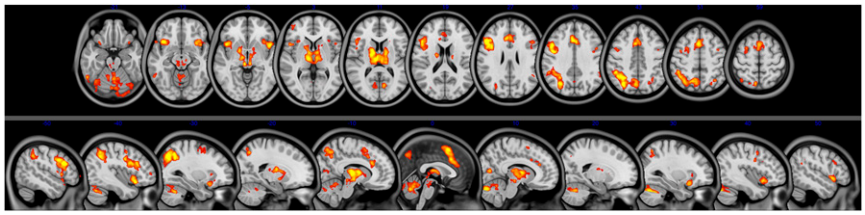

Fig. S4. Incongruent > congruent within-region task activation. Axial (*Upper*; $z = -21$ to 59, slices every 8 mm) and sagittal (*Lower*, $x = -50$ to 50, slices every 10 mm) views of the within-region findings for the incongruent > congruent contrast.

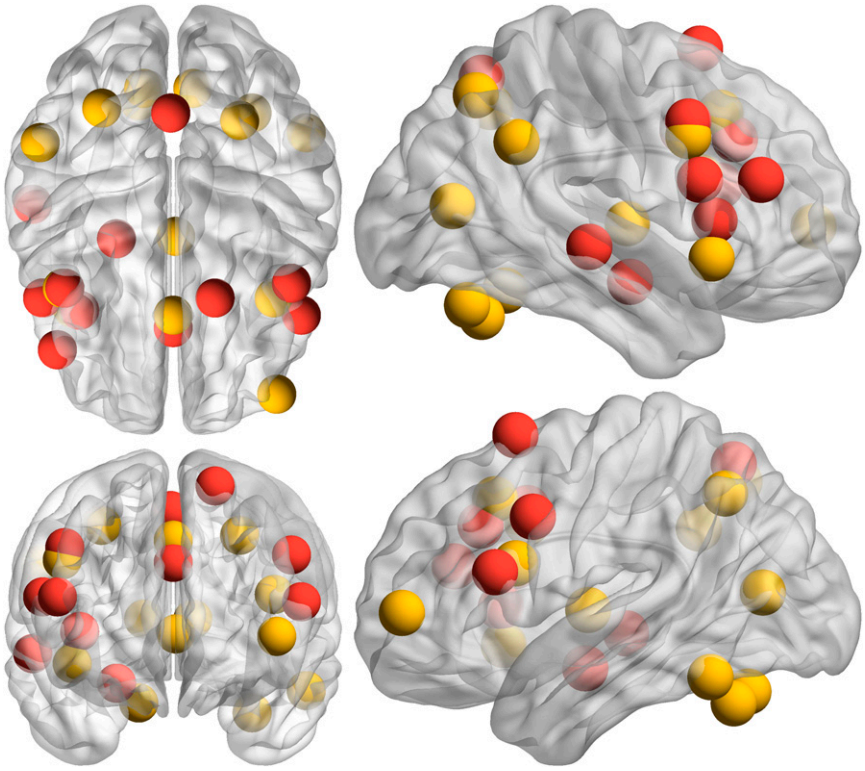

Fig. S5. Overlap of nodes in incongruent > congruent network and within-region task activation. Red spheres are those identified in the network analysis, and yellow spheres are those identified in the within-region task activation analysis. Sphere placement in the brain reflects the center of mass location of that ROI. *Upper Left* is a 3D axial view from above the brain. *Lower Left* is a 3D coronal view from anterior to the brain (to maintain the right side of the brain on the right side of the image for both views, posterior is positioned on top for the axial view). *Upper Right* is a 3D sagittal view from right of the brain. *Lower Right* is a 3D sagittal view from left of the brain.

Table S1. Module membership

Module	Constituent nodes
1	R IFGpo; L & R frontal eye field; L posterior insula/putamen; M mid-cingulate; L & R precentral; R postcentral/precentral; L precentral/superior temporal gyrus; L & R postcentral/superior parietal lobule (×2); R superior temporal gyrus/posterior insula L & R mid-supramarginal; M precuneus; M posterior SFG/MFG; L & R AI; R putamen/globus pallidum; M paracentral (×2); L & R precentral/postcentral; L postcentral; R postcentral/precentral/superior temporal gyrus; L postcentral/inferior parietal lobule; L & R superior temporal gyrus; L & R parietal operculum
2	M anterior paracingulate/medial orbitofrontal cortex; L posterior middle orbitofrontal cortex; L superior temporal gyrus/posterior insula; L & R uncus/temporal pole; R mid-superior temporal gyrus; L mid-middle temporal gyrus; L & R posterior temporal fusiform; L & R hippocampus/amygdala; M subgenual anterior cingulate cortex/medial orbitofrontal cortex; R posterior orbitofrontal cortex/AI; L & R temporal pole/superior temporal gyrus; L & R posterior middle temporal gyrus/superior temporal gyrus; L posterior middle temporal gyrus/superior temporal gyrus; L middle temporal gyrus/superior; temporal gyrus; L lingual
3	L anterior middle orbitofrontal cortex; L & R lateral orbitofrontal cortex/IFG; L & R inferior frontal pole; M anterior SFG; L & R anterior MFG; L & R IFS; L & R mid-SFG/MFG; L posterior SFG/MFG; M pregenual anterior cingulate cortex; M mid-cingulate/posterior cingulate cortex; R superior temporal gyrus/angular; R inferior parietal lobule; L & R superior lateral occipital cortex; R middle orbitofrontal cortex; M frontal pole; R inferior frontal pole; L & R anterior SFG/MFG; M anterior paracingulate gyrus/SFG; L IFGpo; L & R posterior SFG; L & R posterior MFG/precentral; M dACC/paracingulate; M posterior cingulate cortex/precuneus; L angular/superior temporal gyrus/middle temporal gyrus; L inferior parietal lobule/superior parietal lobule; L & R caudate
4	R posterior cingulate cortex/precuneus; M precuneus; R posterior middle temporal gyrus/inferior temporal gyrus; L & R superior lateral occipital cortex (×2); L & R inferior lateral occipital cortex (×2); M cuneus/occipital pole; L occipital pole; L precuneus; R superior lateral occipital cortex/precuneus; L temporal-occipital inferior temporal gyrus; L superior lateral occipital cortex; R lingual; L & R occipital pole/lingual
5	M thalamus/brainstem; M thalamus; L & R ventral striatum; L & R thalamus

L, left; M, medial; R, right; x2, there are two ROIs within the same anatomical area.

Table S2. Incongruent > congruent within-region task activation

Region	Volume, mm^3	Max z	*x*	*y*	*z*
Medial thalamus	23,640	6.61	−2	−12	4
Left angular gyrus/superior lateral occipital cortex/posterior supramarginal gyrus/superior parietal lobule/*medial precuneus	20,344	6.89	−29	−60	44
Left AI/posterior orbitofrontal cortex/*IFGpo/*posterior MFG	18,878	7.21	−42	13	20
Medial *dorsal anterior cingulate/*paracingulate	12,760	6.65	−1	20	42
Right *AI/posterior orbitofrontal cortex	5,320	6.40	40	17	−8
Right *IFGpo/*precentral gyrus	1,465	5.11	44	9	34
Left inferior temporal gyrus, temporooccipital part	1,296	5.38	−55	−54	−19
Right superior parietal lobule/superior lateral occipital cortex	973	5.24	28	−54	48
Right intracalcarine cortex	826	5.62	11	−72	10
Left intracalcarine cortex	507	4.61	−9	−72	10
Right angular gyrus	362	4.67	53	−50	32
Left inferior frontal pole	359	4.92	−43	52	3

Region names correspond to the ROIs used in the network analyses.
*Regions that were also present in the network analyses. *x*, *y*, *z* = coordinates for center of mass.